

Transition of eruptive style: Pumice raft to dome-forming eruption at the Havre submarine volcano, southwest Pacific Ocean

Michael Manga¹, Samuel J. Mitchell², Wim Degruyter³, and Rebecca J. Carey⁴

¹Department of Earth and Planetary Science, University of California, Berkeley, California 94720, USA

²Department of Geology and Geophysics, University of Hawai'i at Manoa, Honolulu, Hawaii 96822, USA

³School of Earth and Ocean Sciences, Cardiff University, Cardiff CF10 3AT, Wales, UK

⁴School of Natural Science and CODES, University of Tasmania, Hobart, Tasmania 7001, Australia

ABSTRACT

Transitions in eruptive style are common at volcanoes. Understanding how and why these transitions occur remain open questions. The 2012 eruption of the submarine Havre volcano in the Kermadec arc (southwest Pacific Ocean) produced a raft of floating pumice followed by a pair of domes from the same vent. Here, we used measurements on erupted magmas and constraints on the eruption rate, combined with a model for magma ascent, to identify the dominant controls on the transition in eruption style. During the raft-forming stage, magma ascent was fast enough that little gas was lost. Magma reached the seafloor with great enough vesicularity to be buoyant and produce clasts that could float. As the eruption waned, the eruption rate decreased, and the conduit narrowed. Sufficient gas was then lost to the surrounding country rocks during ascent such that the erupted magma was no longer buoyant relative to seawater. Most of the original dissolved water in the magma was lost to the crust surrounding the conduit during the dome-forming stage.

INTRODUCTION

Volcanic eruptions commonly transition between different styles, for example, between explosive and effusive eruption. Understanding how and why these transitions occur remain key outstanding questions (National Academies of Sciences, Engineering, and Medicine, 2017) that can provide insight into both ascent processes and hazards (Cassidy et al., 2018). The 2012 silicic submarine eruption of Havre volcano in the Kermadec arc, southwest Pacific Ocean (Fig. 1A), provides a new opportunity to understand transitions in eruptive style. Initially, it created a gigantic raft of floating pumice (Fig. 1B; Jutzeler et al., 2014), and then it extruded a dome on the seafloor from the same vent, 900 m below sea level (Fig. 1C; Carey et al., 2018).

Here, we use a model for magma ascent in a conduit, constrained by measured magma properties, seafloor observations, and eruption constraints, to elucidate the processes governing eruption style. We propose that as the eruption rate decreased during the course of the eruption,

sufficient gas loss during ascent eventually led to magma erupting on the seafloor with vesicularities low enough to be denser than seawater and hence to form a dome.

2012 HAVRE ERUPTION

The 2012 Havre eruption was the largest deep silicic submarine eruption recorded since A.D. 1650 (Jutzeler et al., 2014). On 18 July 2012, more than 1.2 km³ of pumice (bulk volume) reached the ocean surface (Carey et al., 2018), creating a raft of pumice that floated for years and distributed pumice around the Pacific and Southern Ocean basins (Jutzeler et al., 2014).

In March 2015, to better understand this eruption, the Mapping Exploration and Sampling of Havre (MESH) expedition made a high-resolution (1-m-resolution) bathymetric map (Fig. 1C) and collected 290 samples from different locations on the submarine edifice. Submarine exploration of the volcano revealed three clastic pumiceous units, and 15 domes and lavas (Carey et al., 2018). Mapping of stratigraphic

relationships and sampling demonstrated that the vent responsible for the pumice raft is overlain by a 250-m-high, 0.11 km³ pair of domes also erupted in 2012, which we refer to as the OP Dome (Fig. 1C). The OP Dome is unusual in that it is offset from the structural lineament parallel to the southern caldera margin that focused magma in several other locations to form smaller domes (Fig. 1C).

The creation of pumice clasts in subaerial settings is generally attributed to fragmentation processes that lead to an explosive eruption. Manga et al. (2018) showed that the high hydrostatic pressure at the vent allowed sufficient water to remain dissolved in the melt such that the magma viscosity was too low to permit brittle fragmentation in the conduit, and the resulting pumice raft-forming eruption was effusive. Furthermore, Manga et al. (2018) proposed that buoyant magma was extruded into the ocean, where it fragmented upon quenching (van Otterloo et al., 2015) and was then able to float to the ocean surface to supply the pumice raft (Fauria and Manga, 2018).

There remains a key open question: Why did the extruded magma change from being less to more dense than ocean water? The compositions of Dome OP and raft pumice are essentially identical (Table DR1 in the GSA Data Repository¹). The main obvious differences are the vesicularity and texture (Fig. 2): Raft pumice has a mean vesicularity of 78% (Rotella et al., 2015; Carey et al., 2018), and the average of 36 samples from the dome carapace and talus is 39% (Table DR2). While the vesicles are filled with gas, pumice and dome clast densities are less and greater than that of seawater, respectively. The irregular-shaped

¹GSA Data Repository item 2018415, Tables DR1–DR4 and Figure DR5, is available online at <http://www.geosociety.org/datarepository/2018/>, or on request from editing@geosociety.org

CITATION: Manga, M., Mitchell, S.J., Degruyter, W., and Carey, R.J., 2018, Transition of eruptive style: Pumice raft to dome-forming eruption at the Havre submarine volcano, southwest Pacific Ocean: *Geology*, v. 46, p. 1075–1078, <https://doi.org/10.1130/G45436.1>

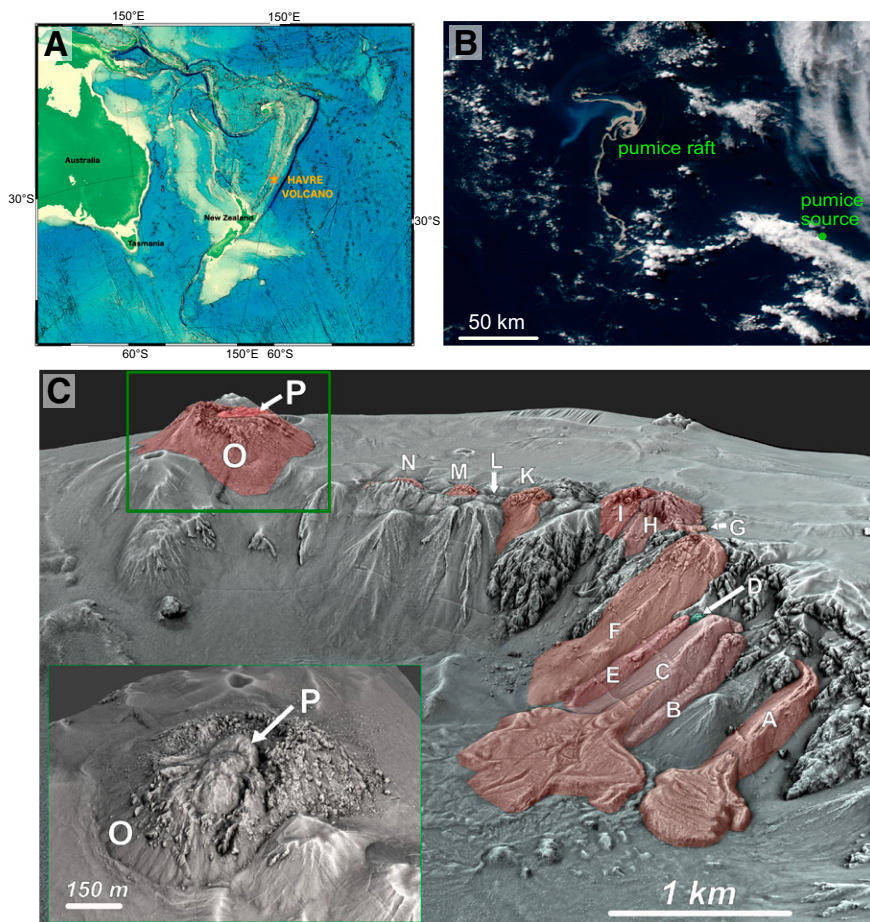


Figure 1. A: Location of Havre volcano in Kermadec arc, southwest Pacific Ocean. **B:** Image of pumice raft, 5 d after eruption. **C:** Map of caldera identifying newly erupted lava flows and domes in red (lettered).

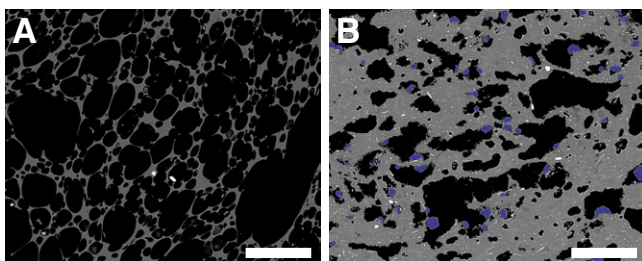


Figure 2. Backscatter electron images of representative clast texture from (A) pumice raft and (B) dome. In B, cristobalite is colored blue. Microlites of plagioclase (white) and pyroxene (dark gray) dominate groundmass in B. Vesicularities are 83 vol% in A and 34.5 vol% in B. Bar in lower right is 100 μm long.

vesicles in the dome samples (Fig. 2B) suggest gas loss and collapse.

ASCENT MODEL

We consider a one-dimensional isothermal and quasi-steady model for magma ascent through a cylindrical conduit of constant radius r following Kozono and Koyaguchi (2012). Two-dimensional models (e.g., Chevalier et al., 2017) permit lateral variations in properties but show qualitatively similar results. Because the phenocryst volume fraction is low, $\sim 5\%$ (Carey et al., 2018), we consider two phases, melt and exsolved water with volume fraction ϕ , and we use subscripts l and g to denote these two phases. We ignore crystallization during ascent, which would act to increase magma viscosity. The mass concentration of dissolved volatiles is c .

We allow the melt velocity u_l and gas velocity u_g to differ, and we permit lateral gas loss through the conduit walls with flux Q_w . Conservation of mass for the melt and gas are, respectively,

$$\frac{d}{dz} \rho_l(1-c)(1-\phi)u_l = 0, \quad (1)$$

$$\frac{d}{dz} [\rho_l c(1-\phi)u_l + \rho_g \phi u_g] = -Q_w, \quad (2)$$

where z is depth. Conservation of momentum, with inertial terms neglected owing to the low Reynolds number, is

$$0 = (1-\phi) \frac{dP}{dz} + \rho_l(1-\phi)g + F_{lw}, \quad (3)$$

$$0 = \phi \frac{dP}{dz} + \rho_g \phi g + F_{lg}, \quad (4)$$

where g is gravity, and F_{lw} and F_{lg} describe the drag forces between magma and the conduit walls and between gas and melt, respectively. The pressure P is assumed to be the same in the gas and melt.

We assume equilibrium outgassing with solubility given by

$$c = s\sqrt{P}. \quad (5)$$

We assume Poiseuille flow of the magma, and thus

$$F_{lw} = \frac{8}{r^2} u_l, \quad (6)$$

and vertical gas loss described by Darcy's law,

$$F_{lg} = \frac{g}{k} \phi^2 (u_g - u_l), \quad (7)$$

with permeability $k = 10^{-11} \phi^3 \text{ m}^2$ (Mueller et al., 2005). Lateral gas loss through the conduit walls is driven by the pressure difference between magma in the conduit P and lithostatic pressure P_l in the surrounding crust (e.g., Jaupart and Allègre, 1991):

$$Q_w = \frac{2\rho_g \phi k_w}{\mu_g r^2} [P - P_l], \quad (8)$$

and it is 0 otherwise, with k_w being the country rock permeability. These models for vertical and lateral volatile loss ignore thermal, multiphase (e.g., liquid vs. vapor), and turbulent effects. The viscosity of the magma, μ_m , varies with dissolved water content, which affects the melt viscosity, μ_l (Manga et al., 2018), and ϕ (Llewellyn and Manga, 2005), such that

$$\mu_m = \left(1 - \phi^{\frac{5}{3}}\right) \mu_l. \quad (9)$$

As boundary conditions, we specify the pressure at the vent (equal to the hydrostatic value at the seafloor depth of 0.9 km) and the mass inflow rate q at the bottom of the conduit. We use $c_0 = 4.9 \text{ wt\%}$ based on melt inclusions from seafloor and raft pumice (mean of 38 inclusions, standard deviation of 0.4 wt%; summarized in Table DR3), temperature $T = 850 \text{ }^\circ\text{C}$ (Manga et al., 2018), and $\rho_l = 2400 \text{ kg/m}^3$, which is also assumed equal to the crust density. We solve for four depth-dependent variables, $P(z)$, $\phi(z)$, $u_l(z)$, and $u_g(z)$, in addition to the "chamber" pressure P_{ch} at the bottom of the conduit. Those variables also determine magma properties such as $\rho_g = P/RT$ and μ_m . We assumed a 5-km-long conduit and solved the coupled differential equations on a regular grid with 5 m spacing (parameters are summarized in Table DR4).

RESULTS

Figure 3 shows the relationship between the mass eruption rate and vesicularity at the vent. We chose these two variables because they are measured (vesicularity) or bounded by observations (eruption rate) for the raft- and dome-forming stages (Carey et al., 2018). We considered two different conduit radii, $r = 30 \text{ m}$ and 12 m ,

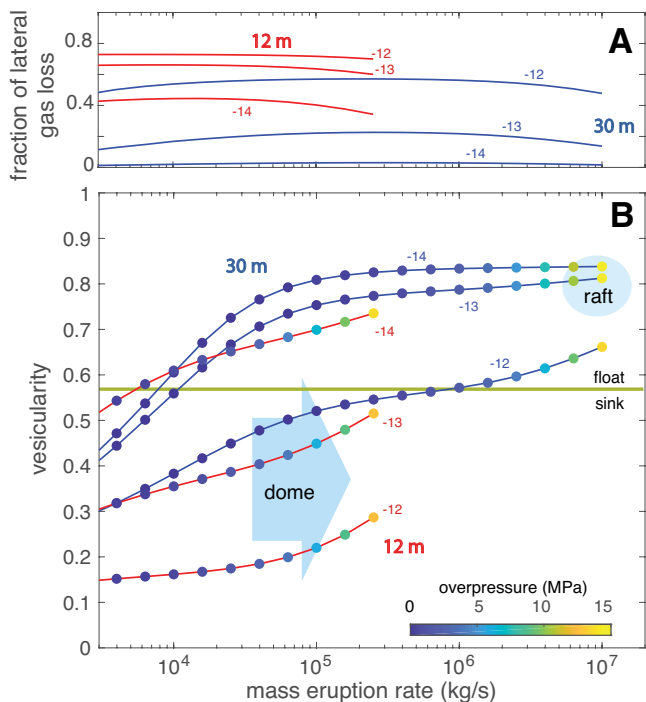


Figure 3. A: Fraction of initial total dissolved water lost to country rocks during ascent. B: Relationship between mass eruption rate and vesicularity at vent. Blue and red curves indicate conduit radii of 30 and 12 m, respectively. Colors of symbols show overpressure at base of conduit (5 km below seafloor). Horizontal line shows vesicularity needed for clasts to be buoyant prior to ingesting liquid water. In A and B, numbers next to each curve are \log_{10} of permeability (in m^2).

and three different wall-rock permeabilities, $k_w = 10^{-14}$, 10^{-13} , and 10^{-12} m^2 , to cover the range typical of upper-crustal rocks (Manning and Ingebritsen, 1999) and oceanic crust (Fisher, 1998).

As the mass eruption rate increases, less gas is lost to the country rock, illustrating “the essential result that the fraction of gas lost is inversely proportional to the eruption rate because the flow of gas occurs at a given rate through the immobile country rock whilst magma rises” (Jaupart and Allègre, 1991, p. 416). At the lowest mass eruption rates shown, vertical gas loss can also reduce vesicularity, even when the crust has a low permeability. However, to achieve vesicularities similar to those of the dome without lateral gas loss, eruption rates are required that are a couple orders of magnitude lower than those calculated at Havre or recorded elsewhere, demonstrating that gas loss to the country rock must have occurred during ascent, and that lateral gas loss (controlled by country rock permeability) likely dominated over vertical gas loss (controlled by magma permeability).

As the conduit radius decreases, the amount of gas lost from the conduit increases. This occurs for two reasons. First, gas flux is inversely proportional to the square of conduit radius (Eq. 8). Second, as conduit size decreases, for the same mass flux, the resistance to ascent (Eq. 6) increases, leading to greater chamber and conduit pressures (colors in Fig. 3) and hence larger pressure differences driving lateral gas loss (Fig. DR5). Vesicularity can increase rapidly as magma approaches the vent owing to both a reduction in the pressure difference between the magma and its surroundings and the increasing ascent speed, which limits the time available for gas loss.

DISCUSSION AND CONCLUSIONS

During the course of an eruption, we expect the overpressure in the magma source to progressively decrease as magma is evacuated (e.g., Woods and Koyaguchi, 1994), leading to a decreasing mass eruption rate. Conduit size can also evolve: Conduit erosion acts to widen ascent paths, but decreasing pressure allows conduits to narrow (e.g., Costa et al., 2007) and cooling and/or crystallization of ascending magma near conduit walls may further decrease the effective conduit size. We ascribe the transition in eruption style at Havre volcano to both evolving magma pressure and decreasing conduit radius. The conduit size was largest during the pumice raft-forming stage of the 2012 Havre eruption, and minimal gas loss occurred during magma ascent because the ascent speed was too high. As the eruption waned, the conduit narrowed, and vertical and lateral gas loss was enhanced (Fig. 4).

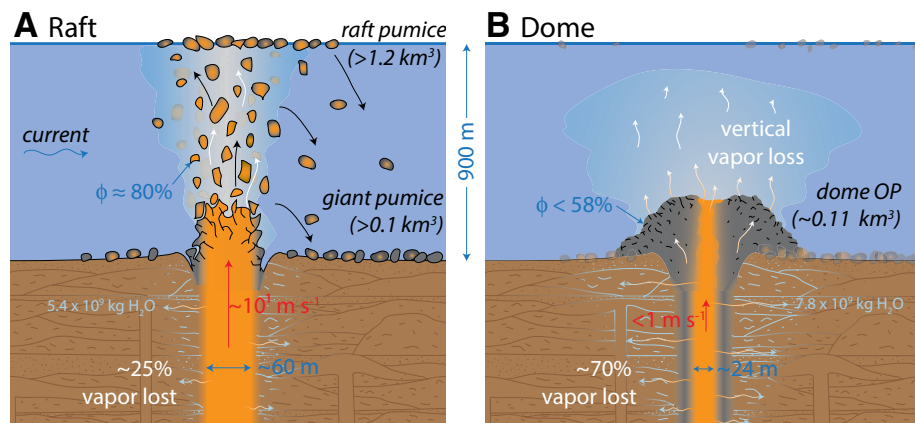


Figure 4. Cartoon illustrating dynamics that accompanied (A) pumice raft-forming eruptions and (B) dome-forming eruptions at Havre volcano (southwest Pacific Ocean) in 2012. Subsurface structure is schematic; ϕ is gas volume fraction.

There are a number of idealizations in the models and uncertainties in the eruption rate data used as inputs. Approximations in our model include a constant permeability for the crust, a cylindrical conduit, and neglect of crystallization. The conduit during the earliest phase of the eruption may well have been more elongate or dike-like, with a shape that evolved over the course of the eruption (e.g., Aravena et al., 2018), but there are no observations to better constrain vent and conduit geometry. The pumice raft samples have a very low abundance of microlites, whereas dome samples have abundant microlites (Fig. 2) that nucleated and grew at some point during ascent or upon emplacement. The eruption rates plotted in Figure 3 are estimates from Carey et al. (2018) based on the mass erupted, constraints on the duration of eruption for the raft, and a lower bound for Dome OP based on 90 d between the raft-forming stage, 18 July 2012, and a comparison of bathymetric surveys on 17 October 2012 and March 2015 that revealed no further growth. This lower bound is within an order of magnitude of the mass eruption rates of recent small-volume rhyolite eruptions at Chaitén and Cerdón Caulle (Pallister et al., 2013; Schipper et al., 2013; Tuffen et al., 2013), but it is considerably less than inferred rates for large-volume rhyolite flows (Befus et al., 2015). The eruption rate might also have decreased monotonically between these estimates for the raft and dome. Nevertheless, the general conclusion that increased gas loss occurs as eruption rate decreases should be robust. A decrease in radius of a factor of ~ 2 combined with a reasonable wall-rock permeability of $\sim 10^{-13} \text{ m}^2$ capture the observed vesicularities and estimates of mass eruption rates. Alternatively, an increasing permeability from 10^{-13} to 10^{-12} m^2 , via fractures in the country rock or volcaniclastic layers, would also explain the changes in vesicularity. We also note that modest vesiculation may have continued as clasts rose in the water column above the vent, increasing raft pumice vesicularity relative

to the values at the vent (Mitchell et al., 2018), which are plotted in Figure 3.

Our explanation for the transition in eruption style requires large volatile fluxes through the magma, particularly during the dome-forming stage. Lateral volatile loss from the conduit to the surrounding rocks is a substantial fraction of the total magmatic volatile budget, ~25% and 70% of the initial water during the raft- and dome-forming stages, respectively (Fig. 3A). Further evidence for high exsolved volatile flux includes the presence of cristobalite in the dome samples (Fig. 2), which likely resulted from vapor-phase crystallization (e.g., Schipper et al., 2017). Given the initial water content of 4.9 wt% and erupted mass of the pumice raft and Dome OP, these values correspond to 5.4×10^9 kg and 7.8×10^9 kg, respectively, of high-temperature supercritical water and vapor supplied to the crust surrounding the conduit. These fluids in hydrothermal systems have the potential to form veins and disseminated mineral deposits within highly altered zones of wall rock surrounding conduits. Syneruptive inputs of magmatic volatiles, fluids, and metals into the shallow (~500 m) seafloor around conduits in deep submarine settings is not considered in classical epithermal or porphyry-style mineralization models (e.g., Large, 1992; Sillitoe and Hedenquist, 2003). Hybrid styles of epithermal–volcanic-hosted massive sulfide–porphyry mineralization have been proposed for both active modern and ancient ore bodies, e.g., Mount Lyell (Yosemite, California; Huston and Kamprad, 2001) and Brothers volcano (South Pacific Ocean; Keith et al., 2018). Greater understanding of these hybrid mineral systems could be attained by geothermal, chemical, and hydrological modeling constrained by quantitative information from Havre volcano.

ACKNOWLEDGMENTS

We thank the Mapping Exploration and Sampling of Havre (MESH) team, remotely and autonomously operated vehicle operators, and the R/V *Roger Revelle* crew for making this science possible. Manga was supported by National Science Foundation (NSF) grant 1521855. Carey was supported by Australian Research Council Postdoctoral fellowships (grants DP110102196 and DE150101190). Carey and Mitchell were supported by NSF grants OCE1357443 and OCE1357216. SIMS analysis was funded by Lipman Research Award GSA12295–18. We thank the reviewers for thoughtful comments, and Fumi Ikegami for help in creating figure 1.

REFERENCES CITED

Aravena, A., Cioni, R., de' Michieli Vitturi, M., Pistolesi, M., Ripepe, M., and Neri, A., 2018, Evolution of conduit geometry and eruptive parameters during effusive events: *Geophysical Research Letters*, v. 45, p. 7471–7480, <https://doi.org/10.1029/2018GL077806>.

Befus, K.S., Manga, M., Gardner, J.E., and Williams, M., 2015, Ascent and emplacement dynamics of obsidian lavas inferred from microlite textures: *Bulletin of Volcanology*, v. 77, p. 88, <https://doi.org/10.1007/s00445-015-0971-6>.

Carey, R., et al., 2018, The largest deep-ocean silicic volcanic eruption of the past century: *Science*

Advances, v. 4, p. e1701121, <https://doi.org/10.1126/sciadv.1701121>.

Cassidy, M., Manga, M., Cashman, K.V., and Bachmann, O., 2018, Controls on explosive-effusive volcanic eruption styles: *Nature Communications*, v. 9, p. 2839, <https://doi.org/10.1038/s41467-018-05293-3>.

Chevalier, L., Collombet, M., and Pinel, V., 2017, Temporal evolution of magma flow and degassing conditions during dome growth, insights from 2D numerical modeling: *Journal of Volcanology and Geothermal Research*, v. 333, p. 116–133, <https://doi.org/10.1016/j.jvolgeores.2017.01.016>, erratum available at <https://doi.org/10.1016/j.jvolgeores.2017.06.008>.

Costa, A., Melnik, O., and Sparks, R.S.J., 2007, Controls of conduit geometry and wallrock elasticity on lava dome eruptions: *Earth and Planetary Science Letters*, v. 260, p. 137–151, <https://doi.org/10.1016/j.epsl.2007.05.024>.

Fauria, K.F., and Manga, M., 2018, Pyroclast cooling and saturation in water: *Journal of Volcanology and Geothermal Research*, v. 362, p. 17–31, <https://doi.org/10.1016/j.jvolgeores.2018.07.002>.

Fisher, A.T., 1998, Permeability within basaltic oceanic crust: *Reviews of Geophysics*, v. 36, p. 143–182, <https://doi.org/10.1029/97RG02916>.

Giordano, D., Russell, J.K., and Dingwell, D.B., 2008, Viscosity of magmatic liquids: A model: *Earth and Planetary Science Letters*, v. 271, p. 123–134, <https://doi.org/10.1016/j.epsl.2008.03.038>.

Huston, D.L., and Kamprad, J., 2001, Zonation of alteration facies at western Tharsis: Implications for the genesis of Cu–Au deposits, Mount Lyell field, western Tasmania: *Economic Geology and the Bulletin of the Society of Economic Geologists*, v. 96, p. 1123–1132, <https://doi.org/10.2113/gsecongeo.96.5.1123>.

Jaupart, C., and Allègre, C.J., 1991, Gas content, eruption rate and instabilities of eruption regime in silicic volcanoes: *Earth and Planetary Science Letters*, v. 102, p. 413–429, [https://doi.org/10.1016/0012-821X\(91\)90032-D](https://doi.org/10.1016/0012-821X(91)90032-D).

Jutzeler, M., Marsh, R., Carey, R.J., White, J.D.L., Talling, P.J., and Karlstrom, L., 2014, On the fate of pumice rafts formed during the 2012 Havre submarine eruption: *Nature Communications*, v. 5, p. 3660, <https://doi.org/10.1038/ncomms4660>.

Keith, M., Haase, K.M., Klemd, R., Smith, D.J., Schwarz-Schampera, U., and Bach, W., 2018, Constraints on the source of Cu in a submarine magmatic-hydrothermal system, Brothers volcano, Kermadec island arc: *Contributions to Mineralogy and Petrology*, v. 173, p. 40, <https://doi.org/10.1007/s00410-018-1470-5>.

Kozono, T., and Koyaguchi, T., 2012, Effects of gas escape and crystallization on the complexity of conduit flow dynamics during lava dome eruptions: *Journal of Geophysical Research—Solid Earth*, v. 117, B08204, <https://doi.org/10.1029/2012JB009343>.

Large, R.R., 1992, Australian volcanic-hosted massive sulfide deposits: Features, styles, and genetic models: *Economic Geology and the Bulletin of the Society of Economic Geologists*, v. 87, p. 471–510, <https://doi.org/10.2113/gsecongeo.87.3.471>.

Llewellyn, E.W., and Manga, M., 2005, Bubble suspension rheology and implications for conduit flow: *Journal of Volcanology and Geothermal Research*, v. 143, p. 205–217, <https://doi.org/10.1016/j.jvolgeores.2004.09.018>.

Manga, M., et al., 2018, The pumice raft-forming 2012 Havre submarine eruption was effusive: *Earth and Planetary Science Letters*, v. 489, p. 49–58, <https://doi.org/10.1016/j.epsl.2018.02.025>.

Manning, C.E., and Ingebritsen, S.E., 1999, Permeability of the continental crust: Implications of

geothermal data and metamorphic systems: *Reviews of Geophysics*, v. 37, p. 127–150, <https://doi.org/10.1029/1998RG900002>.

Mitchell, S.J., McIntosh, I.M., Houghton, B.F., Carey, R.J., and Shea, T., 2018, Dynamics of a powerful deep submarine eruption recorded in H₂O contents and speciation in rhyolitic glass: The 2012 Havre eruption: *Earth and Planetary Science Letters*, v. 494, p. 135–147, <https://doi.org/10.1016/j.epsl.2018.04.053>.

Mueller, S., Melnik, O., Spieler, O., Scheu, B., and Dingwell, D.B., 2005, Permeability and degassing of dome lavas undergoing rapid decompression: An experimental determination: *Bulletin of Volcanology*, v. 67, p. 526–538, <https://doi.org/10.1007/s00445-004-0392-4>.

National Academies of Sciences, Engineering, and Medicine, 2017, *Volcanic Eruptions and Their Repose, Unrest, Precursors, and Timing*: Washington, D.C., National Academies Press, 122 p.

Pallister, J.S., Diefenbach, A.K., Burton, W.C., Muñoz, J., Griswold, J.P., Lara, L.E., Lowenstern, J.B., and Valenzuela, C.E., 2013, The Chaitén rhyolite lava dome: Eruption sequence, lava dome volumes, rapid effusion rates and source of the rhyolite magma: *Andean Geology*, v. 40, p. 277–294, <https://doi.org/10.5027/andgeoV40n2-a06>.

Rotella, M.D., Wilson, C.J., Barker, S.J., Schipper, C.I., Wright, I.C., and Wysoczanski, R.J., 2015, Dynamics of deep submarine silicic explosive eruptions in the Kermadec arc, as reflected in pumice vesicularity textures: *Journal of Volcanology and Geothermal Research*, v. 301, p. 314–332, <https://doi.org/10.1016/j.jvolgeores.2015.05.021>.

Schipper, C.I., Castro, J.M., Tuffen, H., James, M.R., and How, P., 2013, Shallow vent architecture during hybrid explosive-effusive activity at Cordón Caulle (Chile, 2011–12): Evidence from direct observations and pyroclast textures: *Journal of Volcanology and Geothermal Research*, v. 262, p. 25–37, <https://doi.org/10.1016/j.jvolgeores.2013.06.005>.

Schipper, C.I., Mandon, C., Maksimenko, A., Castro, J.M., Conway, C.E., Hauer, P., Kirilova, M., and Kilgour, G., 2017, Vapor-phase cristobalite as a durable indicator of magmatic pore structure and halogen degassing: An example from White Island volcano (New Zealand): *Bulletin of Volcanology*, v. 79, p. 74, <https://doi.org/10.1007/s00445-017-1157-1>.

Sillitoe, R.H., and Hedenquist, J.W., 2003, Linkages between volcanotectonic settings, ore-fluid compositions, and epithermal precious metal deposits, in Simmons, S.F., and Graham, I.J., eds., *Volcanic, Geothermal, and Ore-Forming Fluids: Rulers and Witnesses of Processes within the Earth: Society of Economic Geologists Special Publication 10*, p. 315–343.

Tuffen, H., James, M.R., Castro, J.M., and Schipper, C.I., 2013, Exceptional mobility of an advancing rhyolitic obsidian flow at Cordón Caulle volcano in Chile: *Nature Communications*, v. 4, p. 2709, <https://doi.org/10.1038/ncomms3709>.

van Otterloo, J., Cas, R.A., and Scutter, C.R., 2015, The fracture behaviour of volcanic glass and relevance to quench fragmentation during formation of hyaloclastite and phreatomagmatism: *Earth-Science Reviews*, v. 151, p. 79–116, <https://doi.org/10.1016/j.earscirev.2015.10.003>.

Woods, A.W., and Koyaguchi, T., 1994, Transitions between explosive and effusive eruptions of silicic magmas: *Nature*, v. 370, p. 641–644, <https://doi.org/10.1038/370641a0>.

Printed in USA